UC Irvine
UC Irvine Previously Published Works

Title

A thermo-sensitive fluorescent agent based method for excitation light leakage rejection for fluorescence molecular tomography

Permalink

Journal

Physics in Medicine and Biology, 64(3)

ISSN

0031-9155

Authors

Nouizi, Farouk
Kwong, Tiffany C
Ruiz, Jessica
et al.

Publication Date

2019-02-01

DOI

10.1088/1361-6560/aaf96d

Peer reviewed

A thermo-sensitive fluorescent agent based method for excitation light leakage rejection for fluorescence molecular tomography

Farouk Nouizi[1], **Tiffany C Kwong**[1], **Jessica Ruiz**[1], **Jaedu Cho**[1], **Yu-Wen Chan**[1], **Kenji Ikemura**[2], **Hakan Erkol**[3], **Uma Sampathkumaran**[4], **Gultekin Gulsen**[1]

[1]Department of Radiological Sciences, Tu and Yuen Center for Functional Onco-Imaging, University of California, Irvine, CA 92697, United States of America

[2]Department of Pathology, Montefiore Medical Center, Albert Einstein College of Medicine, Bronx NY, United States of America

[3]Department of Physics, Bogazici University, 34342 Bebek, Istanbul, Turkey

[4]InnoSense LLC, 2531 West 237th Street, Suite 12, Torrance, CA 90505, United States of America

Abstract

Fluorescence molecular tomography (FMT) is widely used in preclinical oncology research. FMT is the only imaging technique able to provide 3D distribution of fluorescent probes within thick highly scattering media. However, its integration into clinical medicine has been hampered by its low spatial resolution caused by the undetermined and ill-posed nature of its reconstruction algorithm. Another major factor degrading the quality of FMT images is the large backscattered excitation light component leaking through the rejection filters and coinciding with the weak fluorescent signal arising from a low tissue fluorescence concentration. In this paper, we present a new method based on the use of a novel thermo-sensitive fluorescence probe. In fact, the excitation light leakage is accurately estimated from a set of measurements performed at different temperatures and then is corrected for in the tomographic data. The obtained results show a considerable improvement in both spatial resolution and quantitative accuracy of FMT images due to the proper correction of fluorescent signals.

Keywords

fluorescence molecular tomography; excitation light leakage; biomedical imaging; optical imaging

1. Introduction

Fluorescence molecular tomography (FMT) is an emerging molecular imaging modality which is capable of providing quantitatively accurate 3D distributions of endogenous or exogenous fluorescent probes in thick highly scattering media (Ntziachristos 2006,

fnouizi@uci.edu.

Venugopal *et al* 2010, Lin *et al* 2010b, Darne *et al* 2013, Rice *et al* 2015). FMT has become an important tool in preclinical oncology research due to its ability to noninvasively resolve the metabolic processes of fluorescent probes and biomarkers in bio-tissue (Kossodo *et al* 2010, Ale *et al* 2012, Ma *et al* 2017, Zhang *et al* 2018). Despite using non-ionizing radiation and low-cost instrumentation, the integration of FMT into clinical medicine has been hampered by its low spatial resolution caused by the undetermined and ill-posed nature of its image reconstruction algorithm (Arridge 1999, Lihong and Wang 2007, Leblond *et al* 2010). Furthermore, the quality of the images reconstructed by FMT is highly sensitive to the signal to noise ratio (SNR) (Hwang *et al* 2005, Marshall *et al* 2010, Sevick-Muraca 2012, Sexton *et al* 2013).

The majority of the noise affecting FMT measurements arises from the spectral contribution of the excitation light leaking through the rejection filters due to their limited performance (Lu *et al* 2011). To fully take advantage of the high sensitivity of FMT, the elimination of the excitation light leakage component from the measured signals is crucial (Zhu *et al* 2010). In fact, acquiring accurate fluorescence signals strongly depends on the ability to correct for this limitation especially when the tissue fluorescence concentration is low or when the fluorescent probes accumulate deep in the tissue. The excitation light leakage component can be eliminated up to a certain degree by incorporating a combination of notch, long-pass, and band-pass filters. However, the performance of these rejection filters is limited when the incident light penetrates the surface of the filter at an angle from its normal (Zhu *et al* 2010). This is observed when camera based non-contact systems are used, where the lens combination is not ideal such that light is not collimated when it passes through the rejection filters (Hwang *et al* 2005, Nouizi *et al* 2015b). Therefore, even with the use of the best rejection filters combination, it is crucial to account for the contribution of excitation light leakage and correct for it, in order to obtain high quantification and spatial resolution FMT images (Roy and Sevick-Muraca 1999a, 1999b, Eppstein *et al* 2002, Hwang *et al* 2005, Soubret and Ntziachristos 2006, Davis *et al* 2008, Liu *et al* 2012, Tichauer *et al* 2013, Fantoni *et al* 2014, 2015).

For phantom or pharmacokinetic studies, a common solution for excitation light leakage suppression consists in the subtraction of the measurements performed before the injection of the fluorescent agent (pre-injection excitation light leakage measurements) from the measurements acquired after the injection under the same experimental configurations and settings (Hwang *et al* 2006, Lu *et al* 2011, Tichauer *et al* 2012, Davis *et al* 2013). This method is referred to as '*Standard method*' in this paper. It is only valid for phantom studies or while studying kinetics, where images are acquired immediately before and after the injection of the fluorescent contrast agent. It also assumes that the imaged animal remains stationary as the quality of the corrected measurements using this method highly depends on the ability to immobilize the animal during this period between the two data acquisitions (Zhang *et al* 2018). Moreover, keeping the same experimental settings for both measurements is an additional challenge as gain settings are set only when the fluorescent agent is injected (Lin *et al* 2012a). In addition, when using targeted fluorescent probes that require a long circulation period, generally over 10 h, to accumulate in tumours, this method is useless due to the difficulty of replicating the exact same experimental settings to acquire before and after injection data (Ardeshirpour *et al* 2014, 2018).

In this paper, we propose a new method that allows an effective excitation light leakage suppression even after injection of the fluorescent agent which makes it suitable for small animals imaging even when targeted fluorescence probes are used (Nouizi *et al* 2015b). Our method is based on the use of the recently emerged thermo-sensitive fluorescence probe (ThermoDots) consisting of ICG-loaded pluronic nanocapsules (Kim *et al* 2010, Chen and Li 2011, Kwong *et al* 2015). The quantum efficiency and lifetime of these ThermoDots are sensitive to temperature variations (Lin *et al* 2012b, Nouizi *et al* 2015a). Taking advantage of this property, two methods allowing the estimation of the excitation light leakage are presented. The reconstructed images using these corrected measurements are compared to the images reconstructed using raw data and data corrected using the aforementioned *Standard method*.

2.   Materials and methods

2.1.   Instrumentation

FMT measurements in this study were performed using the experimental setup illustrated in figure 1. The system consists of a conventional CCD based fluorescence reflection tomography scanner. Illumination of the imaged phantom was performed using a 785 nm laser diode (300 mW, Thorlabs, Newton, NJ). The selection of the laser wavelengths was based on the optical property of our ThermoDots (Kwong *et al* 2015). Similar to indocyanine green (ICG), the ThermoDots were characterized and found to have a maximum excitation and emission spectra at 785 nm and 830 nm, respectively. The laser was focused before it was sent to the galvano-mirrors which were programmed to automatically scan the phantom using a point source scheme (Nouizi *et al* 2015b). The detection of the emitted fluorescence signal was performed using a cooled CCD camera (Perkin Elmer, Cold Blue) coupled to a sigma MACRO 50 mm F2.8 lens. Acquisition of a clean fluorescence signal requires applying adequate rejection filters with the appropriate optical density in order to separate the strong backscattered excitation light from the weak fluorescence signal. A computer-controlled filter wheel (Tofra, Inc.) was installed between the CCD camera body and the lens. In the following study, two 830 nm band-pass filters (MK Photonics) were cascaded to decrease the leakage of the excitation light. A Labview software (National Instruments, Austin, TX) was used to control each component and to perform the automatic data acquisition. A heating pad was placed under the phantom to heat and maintain a stable temperature during the study as well. The temperature was monitored using a thermocouple (Photon Control, Inc.), placed inside the tube containing the ThermoDots, Fig 1.

2.2.   Phantom design

The phantom used in this study is a rectangular $47 \times 62 \times 20$ mm^3 agarose gel phantom, figures 1(b) and (c). Intralipid (0.5%) and Indian ink were added to agar to set the absorption and reduced scattering coefficients of the phantom to be 0.0132 mm^{-1} and 0.8 mm^{-1}, respectively. The origin of the spatial coordinates was set to be at the top right corner of the phantom. Two 5 mm inner diameter glass tubes were buried 10 mm below the upper surface along the *x*-axis with tube 1 at $y = 21$ mm and tube 2 at $y = 41$ mm, figures 1(b) and (c).

2.3. ThermoDots (ICG-loaded pluronic nanocapsules)

The ThermoDots were prepared by our industrial collaborator, *InnoSense LLC* (USA). ThermoDots consist of ICG encapsulated in Pluronic-F127 polymeric micelles (Kwong *et al* 2015, 2017). They were characterized to determine their thermo-responsiveness and active temperature ranges. For these phantom studies, ThermoDots were optimized to perform between 14 °C and 24 °C. Within this operating range, the intensity of the emitted fluorescence signal increases approximately 10-fold. Details on ThermoDots preparation and characterization can be found in Kwong *et al* (2015).

2.4. Leakage suppression

Let $M_{sd}(T)$ be the fluorescence signal measured at temperature T when the source s and the detector d are used. Taking into consideration that the excitation light leakage (L_{sd}) is independent of temperature, the fluorescence signal measured at a given temperature T_i can be written as:

$$M_{sd}(T_i) = f_{sd}(T_i) + L_{sd} \tag{1}$$

where $f(T_i)$ is the theoretical fluorescence signal at temperature T_i. Performing measurements at two different temperatures, $T_2 > T_1$ and $\eta(T_2) > \eta(T_1)$, equation (1) can be written as:

$$\begin{cases} M_{sd}(T_1) = f_{sd}(T_1) + L_{sd} \\ M_{sd}(T_2) = f_{sd}(T_2) + L_{sd} = (1 + \alpha)f_{sd}(T_1) + L_{sd} \end{cases} \tag{2}$$

where the parameter α defines the variation of the fluorescence signal due to the temperature increase:

$$\alpha = \frac{\eta(T_2)}{\eta(T_1)}, \quad \eta(T_1) > 0. \tag{3}$$

Based on the linear relationship between the fluorescence signal and the quantum yield of fluorescence, α can be also obtained by the ratio of the signals $M_{s,d}(T)$, $T = T_1, T_2$.

2.4.1. Method 1: low temperature, $\eta(T_{low}) \approx 0$—The advantage of using
ThermoDots is that their operating temperature range can be tunable allowing us to obtain a very low fluorescent signal $f(T_b) \approx 0$, at low temperature $T = T_{low}$. At this temperature, the measured signal consists essentially of the excitation light leakage component such that:

$$L_{sd} = M_{sd}(T_{low}). \tag{4}$$

The leakage measured using this method is referred to as $Leak_1$ in this paper. Thus, the corrected fluorescence signal at any temperature T_i is derived from equation (2) and can be written as:

$$f_{sd}(T_i) = M_{sd}(T_i) - L_{sd} = M_{sd}(T_i) - M_{sd}(T_{low}). \tag{5}$$

The operating temperature range of the ThermoDots is usually tuned to have a quasi null emission at body temperature when performing animal imaging. By this way, the leakage is obtained by simply acquiring one set of data before heating.

2.4.2.   Method 2: $T_2 > T_1 > T_{low}$ and $\eta(T_i) > 0$—In the case where it is not possible to obtain the data at a low temperature, the excitation light leakage can still be corrected for by performing a set of two measurements at two different temperatures, $T_2 > T_1$ and $\eta(T_2) > \eta(T_1)$. The excitation light leakage can be expressed as a function of two measured signals at these two different temperatures $M_{sd}(T_2) > M_{sd}(T_1)$, and the variation of the fluorescence signal due to the temperature increase, α, takes the following form by using equations (2) and (3):

$$L_{sd} = \frac{(1+\alpha)M_{sd}(T_1) - M_{sd}(T_2)}{\alpha}. \tag{6}$$

The leakage estimated using this method is referred to as $Leak_2$ in this paper. The corrected fluorescence signal at any temperature T_i is then obtained by simply subtracting the leakage L_{sd} estimated by equation (6).

2.5.   FMT image reconstruction framework

Reconstruction of the FMT images is a two-step process. The first step is the resolution of the forward problem which consists of modeling the propagation of the excitation light from the illumination site at the surface of the imaged medium to the fluorophore, then modeling the fluorescence light emitted from the fluorophore to the surface of the medium (Arridge 1999, Nouizi *et al* 2009, Ducros *et al* 2010, Lin *et al* 2015). It has been established and generally accepted that the diffusion equation is an adequate tool to model the light transport in highly scattering media (Arridge 1999, Erkol *et al* 2015, Nouizi *et al* 2016a, 2016b). Generally, the intensity of emitted fluorescence signal is independent of the temperature of the medium when using conventional fluorescent probes (Gao *et al* 2010, Laidevant *et al* 2011). However, the fluorescence signal is highly temperature dependent when using our ThermoDots due to the thermo-sensitivity of their quantum efficiency and lifetime (Lin *et al* 2012b). The density of fluorescence photons Φ_m^T within the medium at a temperature T is given by Nouizi *et al* (2015a, 2015b), Lin *et al* (2015) and Kwong *et al* (2017):

$$\begin{cases} -\nabla[D_x \nabla \Phi_x] - [\mu_{af} + \mu_{ax}]\Phi_x = -q_0 \\ -\nabla\left[D_m \nabla \Phi_m^T[\eta(T)]\right] - \mu_{am}\Phi_m^T[\eta(T)] = -\Phi_x \eta(T)\mu_{af} \end{cases} \tag{7}$$

where q_0 is the source of the excitation light. D is the diffusion coefficient and μ_a corresponds to the absorption coefficient. The subscripts x and m represent the excitation and emission wavelengths, respectively. Φ_x is the density of excitation photons. η is the temperature dependent quantum yield of fluorescence and μ_{af} is the fluorescence absorption coefficient.

The second step is generally referred to as the inverse problem, which consists in minimizing the quadratic error between the measured and the simulated data (Arridge 1999).

The minimization is performed using the Levenberg–Marquardt method, where the unknown μ_{af} distribution is iteratively updated by Lin *et al* (2010a):

$$\mu_{af}^{m+1} = \mu_{af}^{m} + \left[J^T J + \lambda I \right]^{-1} J^T \left[M - F\left(\mu_{af}^{m}\right) \right] \tag{8}$$

where F is the forward problem operator used to generate the simulated data and M is the experimentally measured data. J is the Jacobian matrix calculated using the adjoint-method (Arridge 1999). λ is the regularization parameter and I is the identity matrix.

3.   Results and discussion

3.1.   ThermoDots characterization

After synthesizing the ThermoDots, they first need to be characterized to be able to generate quantitatively accurate FMT images within the tissue. The characterization of the ThermoDots consists mainly in defining their temperature operating range, and their fluorescence quantum yield for all temperatures within the operating range. Extensive details on the characterization of ThermoDots and the dedicated photomultiplier-based system were presented by Kwong *et al* (2015). Briefly, this involved comparing the intensity of the fluorescence light emitted from the ThermoDots with a known concentration of ICG solution as the temperature was increased gradually.

In the following section, we chose to present a more visual characterization technique using the same reflectance FMT CCD system and phantom to be used later in this paper, figure 1(a). This technique simply consisted in filling the two tubes with different fluorescent probes and comparing the emitted fluorescence light reaching the upper surface of the phantom. In this technique, it is essential that the excitation light point source is exactly midway between the two tubes. To determine the exact position of this midway point source, both tubes were filled with a solution with 5 μMol of ICG, figure 2(a). The laser point source was then scanned between the two tubes, along the y-axis at $x = 18$ mm, until the fluorescence signals emitted from both tubes had equal intensities as can be seen on the profile (green line with + marker) performed at the surface of the phantom, figure 2(b). The profile consisted of two main diffused fluorescence peaks above the two tubes and a sharp backscattered peak at the position of the excitation source.

After the determination of the central point between the two tubes, tube 2 was filled with ThermoDots in order to find the fluorescence quantum yield by comparing the ThermoDots fluorescence light emission at different temperatures to a 5 μMol ICG solution. The phantom was then placed on top of the heating pad in the field of view of the CCD, figure 1(a). For this experiment, the initial temperature of the phantom was 14 °C and was gradually increased to 24 °C using the heating pad. The temperature of ThermoDots was monitored using a thermocouple placed inside tube 2. The fluorescence images were acquired using the CCD camera with an integration time set to 2 s. The baseline fluorescence image was first acquired at 14 °C then a single image was acquired after each 1 °C increase, resulting in 11 fluorescence images.

The obtained results are presented as profiles carried-out along the *y*-axis at $x = 18$ mm on the fluorescence images, figure 2(b). At low temperature, we were only able to observe the peak above tube 1 containing ICG (green highlighted area). This was because the quantum yield of ThermoDots in tube 2 was tuned to be sufficiently low yielding almost no fluorescence emission at this temperature. By gradually increasing the temperature of the phantom, the peak above tube 2 (red highlighted area) displayed a gradual increase as opposed to the first peak above tube 1 containing the ICG solution. The temperature independence of the excitation light leakage was shown as its peak intensity remained constant during the experiment, figure 2(b). The signal increase was quantified by integrating the fluorescence signals above tube 2, between $y = 35$ mm and $y = 50$ mm. The blue curve in figure 2(c) shows the results obtained after normalizing the obtained intensities by the baseline intensity observed at 14 °C when no fluorescence was emitted from tube 2. The baseline signal observed above tube 2 at this temperature was essentially composed of the tails of the excitation light peak and the fluorescent peak above tube 1 since the ThermoDots emission was tuned to be negligible. In order to be able to compare this curve with the invariant intensity obtained above the tube containing ICG, this was later normalized using the same baseline obtained from the ThermoDots, figure 2(c). Based on the linear relationship between the fluorescence quantum yield and the intensity of fluorescence light, the fluorescence quantum yield of the ThermoDots and ICG solution were considered equal when both intensities of the emitted light were equal. By interpolation, figure 2(c) shows that the fluorescence quantum yield of the ThermoDots and ICG solution were equal when the temperature reached 17.1 °C. This value will be used as reference in the definition of the fluorescence quantum yield of the ThermoDots at any temperature. The quantum yield at all other temperatures within the operating range can be obtained using a linear interpolation of the relative increase of the fluorescence emitted light, figure 2(c).

3.2. Excitation leakage estimation and correction

For both methods, fluorescence signals needed to be acquired at two different temperatures. For method 1, fluorescence signals were first acquired at a low temperature where the emission of ThermoDots was negligible, then acquired at a higher temperature. Method 2 was more practical and required a set of two fluorescence signals acquired at any temperature yielding a non-negligible emission of the ThermoDots.

A second phantom with the same geometry, but with the absorption and reduced scattering coefficients respectively increased by a factor of 2 and 1.5, was used to emphasize the importance of excitation light leakage correction. Here, only tube 2 was used and filled with our ThermoDots. Tube 1 was filled with a solution with identical optical properties of the phantom. The fluorescence signals were acquired at three different temperatures: (1) $T_1 = 15$ °C to mimic a low temperature where the fluorescence emission of ThermoDots is negligible, (2) $T_2 = 17$ °C which is the temperature where the emission is equivalent to ICG, and finally (3) $T_3 = 19$ °C to mimic an increase of 2 °C, which is tolerable when performing small animal imaging.

In order to compare our results with the *Standard method* that consists in measuring the leakage before the injection of the fluorescent probe, an additional set of data was acquired by removing the ThermoDots from tube 2 and replacing it with an intralipid solution having the same optical properties as the phantom, similar to tube 1.

All the reflectance fluorescence images were acquired using a 2 s integration time. In figure 3, Standard shows the fluorescence image containing only the leakage component measured using the *Standard method* where no fluorescent agent was present in the phantom. In figure 3, 15 °C, 17 °C, 19 °C show the images acquired at $T_1 = 15$ °C, $T_2 = 17$ °C and $T_3 = 19$ °C, respectively. The profiles presented in the second row of figure 3 clearly show the variation of the fluorescent signal intensity above tube 2 due to the temperature increase.

The leakage was first measured using the *Standard method* and then estimated using method 1 (*Leak₁*), and method 2 (*Leak₂*). In figure 4, Standard, *Leak₁*, and *Leak₂* show the leakage obtained using: the *Standard method*, method 1 (*Leak₁*), and method 2 (*Leak₂*), respectively. The profiles presented in figure 4 show that both method 1 and 2 provided a similar good estimate of the excitation leakage when compared to the leakage measured using the *Standard method*. A weak residual signal can be noticed above tube 2 due to the error in the temperature measurement. The temperature was held constant with standard deviation of 0.27 °C using the heating pad during the acquisition of the fluorescence data. In future works, a closed loop control of temperature would be used to obtain better results.

The fluorescence signals were corrected by simply subtracting the estimated leakage signals obtained using one of the three methods presented above, figure 4. As an example, figure 5 shows the fluorescence signals acquired at $T_3 = 19$ °C corrected by subtracting the obtained excitation leakage. The corrected data only showed the fluorescence component above tube 2 containing the ThermoDots. In fact, the images showed that the excitation leakage component has been efficiently corrected for, with a residual error less than 1% of the removed excitation leakage peak.

4. FMT image reconstruction

The FMT data acquired at T_3 presented the best SNR and was used to validate our method to improve FMT image quality. Tomographic data was acquired by scanning the excitation light source point along the *y*-axis, $x = 18$ mm, at 9 equidistant positions between $y = 6$ mm and $y = 56$ mm. As aforementioned, obtaining quantitatively accurate FMT images requires the determination of the quantum yield of fluorescence of the ThermoDots and the temperature at which data was acquired. At $T_3 = 19$ °C, the fluorescence quantum yield of ThermoDots (η_T) was higher than the 5 μMol ICG solution (η_{ICG}). Using the curve on figure 2(c), we obtained $\eta_T = 3.28 \ \eta_{ICG}$ at T_3.

Four reconstructions were performed using the raw data (**Raw**) and the data was corrected using: *Standard method* (Standard), method 1 (***Leak₁***), method 2 (***Leak₂***). An additional reconstruction was also performed using simulated data to be used as gold standard for the evaluation of the quality of the reconstructed images. This simulated data was generated

using the fluorescence quantum yield of the ThermoDots at 19 °C and the geometry and optical properties of the phantom.

The reconstructions were performed on a rectangular mesh consisting of 1262 nodes which formed 2363 triangular elements. All reconstructions were started using the same homogeneous initial guess. The reconstruction algorithm was automatically stopped when the resulting reconstruction error did not show an improvement superior to 5% during three successive iterations. Figure 6 shows the obtained reconstructions. The reconstructed image using the simulated data (**Simu**) shows that even when using ideal data, the target was reconstructed 2.5 mm closer to the surface due to the reflection data acquisition scheme. The reconstructed image using the raw data (**Raw**) shows multiple artefacts due to the presence of the excitation light leakage contaminating the data. This image showed the lowest estimation of the fluorescence absorption of all five reconstructed images. The last three reconstructed images, Standard, $Leak_1$ and $Leak_2$ showed similar results to those obtained using the simulated data. The higher spatial resolution of these images, obtained using the corrected data (Standard, $Leak_1$ and $Leak_2$) demonstrated the necessity for the correction of the excitation light leakage.

In order to compare the quality of the obtained images, the medium was divided into two regions: background and inclusion. As aforementioned, the inclusion was reconstructed 2.5 mm closer to the upper surface of the phantom. Therefore, the quantification was not performed within the real inclusion boundary (Real) but within the boundary segmented at full width half maximum of the image reconstructed using the simulated data (Simu). The mean value and standard deviation of the obtained fluorescence absorption are summarized in table 1.

Figure 6, (1)–(3) show the profiles along the three lines defined by the three arrows on the image Raw. The profiles are computed on the images: Real, Simu, Raw and only $Leak_2$ as the profiles obtained from the images Standard and $Leak_1$ were nearly identical to the ones obtained from $Leak_2$. The intensity of fluorescence obtained with the corrected data was very similar to the one obtained using simulated data and was 30% higher than the one obtained when using the raw data. These results clearly show how the correction for the excitation light leakage has a significant improvement in the reconstructed images. The data correction not only reduced the reconstruction artefacts but improved the quantitative estimation of the fluorescence absorption as well.

5. Conclusion

The quantitative and spatial quality of FMT highly depends on the quality of the fluorescence signals acquired at the surface of the imaged tissue. In general, these signals are contaminated with other signals originating mainly from the excitation light leakage through the rejection filters. This leakage is several orders of magnitude higher than the fluorescence signal of interest, which is highly dependent on the fluorescent probe concentration and depth within the tissue. Therefore, there is a crucial need for the correction of the excitation light leakage, which is present in the measurements even with

the use of an ideal combination of lens to focus and collimate the light into multiple rejection interference filters.

This correction is a straightforward step where excitation light leakage is simply measured before introducing the fluorescence probe within the phantom then subtracted from the fluorescence measurements. This method remains valid while studying fluorescence probes pharmacokinetics, where the images are obtained immediately before and after the injection of the fluorescent contrast agent. However, the quality of the corrected measurements highly depends on the ability to immobilize the animal during this period between the two data acquisitions. In addition, a long circulation period is required when using targeted fluorescent probes, which makes this method useless due to the impossibility of replicating the same experimental settings to acquire before and after injection data.

In this contribution, we demonstrate a new method for post-imaging excitation light leakage estimation from a set of measurements obtained using our thermo-sensitive fluorescence probes (ThermoDots) at different temperatures. In fact, our method is equivalent to performing measurements before and after fluorescent agent injection. Nevertheless, our method overcomes the challenging step of 'before and after imaging' data acquisition allowing us to perform excitation light leakage estimation at anytime even after the injection of the ThermoDots.

Acknowledgment

References

Ale A, Ermolayev V, Herzog E, Cohrs C, de Angelis MH and Ntziachristos V 2012 FMT-XCT: *in vivo* animal studies with hybrid fluorescence molecular tomography-x-ray computed tomography Nat. Methods 9 615 [PubMed: 22561987]

Ardeshirpour Y, Chernomordik V, Hassan M, Zielinski R, Capala J and Gandjbakhche A 2014 *In vivo* fluorescence lifetime imaging for monitoring the efficacy of the cancer treatment Clin. Cancer Res 20 353120139

Ardeshirpour Y, Sackett DL, Knutson JR and Gandjbakhche AH 2018 Using *in vivo* fluorescence lifetime imaging to detect HER2-positive tumors EJNMMI Res. 8 26 [PubMed: 29619584]

Arridge S 1999 Optical tomography in medical imaging Inverse Problems 15 R41–93

Chen Y and Li X 2011 Near-infrared fluorescent nanocapsules with reversible response to thermal/pH modulation for optical imaging Biomacromolecules 12 4367–72 [PubMed: 22040128]

Darne C, Lu Y and Sevick-Muraca EM 2013 Small animal fluorescence and bioluminescence tomography: a review of approaches, algorithms and technology update Phys. Med. Biol 59 R1–64 [PubMed: 24334634]

Davis SC, Pogue BW, Springett R, Leussler C, Mazurkewitz P, Tuttle SB, Gibbs-Strauss SL, Jiang SS, Dehghani H and Paulsen KD 2008 Magnetic resonance—coupled fluorescence tomography scanner for molecular imaging of tissue Rev. Sci. Instrum 79 064302–10 [PubMed: 18601421]

Davis SC, Samkoe KS, Tichauer KM, Sexton KJ, Gunn JR, Deharvengt SJ, Hasan T and Pogue BW 2013 Dynamic dual-tracer MRI-guided fluorescence tomography to quantify receptor density *in vivo* Proc. Natl Acad. Sci 110 9025–30 [PubMed: 23671066]

Ducros N, D'Andrea C, Valentini G, Rudge T, Arridge S and Bassi A 2010 Full-wavelet approach for fluorescence diffuse optical tomography with structured illumination Opt. Lett 35 3676–8 [PubMed: 21042388]

Eppstein MJ, Hawrysz DJ, Godavarty A and Sevick-Muraca EM 2002 Three-dimensional, Bayesian image reconstruction from sparse and noisy data sets: near-infrared fluorescence tomography Proc. Natl Acad. Sci. USA 99 9619–24 [PubMed: 12105269]

Erkol H, Nouizi F, Luk A, Unlu MB and Gulsen G 2015 Comprehensive analytical model for CW laser induced heat in turbid media Opt. Express 23 31069–84 [PubMed: 26698736]

Fantoni F, Hervé L, Poher V, Gioux S, Mars JI and Dinten J-M 2014 Laser line scanning for fluorescence reflectance imaging: a phantom study and *in vivo* validation of the enhancement of contrast and resolution J. Biomed. Opt 19 106003 [PubMed: 25271541]

Fantoni F, Hervé L, Poher V, Gioux S, Mars J and Dinten J-M 2015 Laser line illumination scheme allowing the reduction of background signal and the correction of absorption heterogeneities effects for fluorescence reflectance imaging J. Biomed. Opt 20 106003 [PubMed: 26442963]

Gao F, Li J, Zhang L, Poulet P, Zhao H and Yamada Y 2010 Simultaneous fluorescence yield and lifetime tomography from time-resolved transmittances of small-animal-sized phantom Appl. Opt 49 3163–72 [PubMed: 20517387]

Hwang K, Houston JP, Rasmussen JC, Joshi A, Ke S, Li C and Sevick-Muraca EM 2005 Improved excitation light rejection enhances small-animal fluorescent optical imaging Mol. Imaging 4 194–204 [PubMed: 16194451]

Hwang K, Pan T, Joshi A, Rasmussen JC, Bangerth W and Sevick-Muraca EM 2006 Influence of excitation light rejection on forward model mismatch in optical tomography Phys. Med. Biol 51 5889–902 [PubMed: 17068371]

Kim TH, Chen Y, Mount CW, Gombotz WR, Li X and Pun SH 2010 Evaluation of temperature-sensitive, indocyanine green-encapsulating micelles for noninvasive near-infrared tumor imaging Pharm. Res 27 1900–13 [PubMed: 20568000]

Kossodo S, Pickarski M, Lin S-A, Gleason A, Gaspar R, Buono C, Ho G, Blusztajn A, Cuneo G and Zhang J 2010 Dual *in vivo* quantification of integrin-targeted and protease-activated agents in cancer using fluorescence molecular tomography (FMT) Mol. Imaging Biol 12 488–99 [PubMed: 19960268]

Kwong TC, Nouizi F, Lin Y, Cho J, Zhu Y, Sampathkumaran U and Gulsen G 2017 Experimental evaluation of the resolution and quantitative accuracy of temperature-modulated fluorescence tomography Appl. Opt 56 521–9 [PubMed: 28157909]

Kwong TC, Nouizi F, Sampathkumaran U, Zhu Y, Alam MM and Gulsen G 2015 Activatable thermo-sensitive ICG encapsulated pluronic nanocapsules for temperature sensitive fluorescence tomography Proc. SPIE 9339 93390C

Laidevant A, Hervé L, Debourdeau M, Boutet J, Grenier N and Dinten JM 2011 Fluorescence time-resolved imaging system embedded in an ultrasound prostate probe Biomed. Opt. Express 2 194–206

Leblond F, Davis SC, Valdes PA and Pogue BW 2010 Pre-clinical whole-body fluorescence imaging: Review of instruments, methods and applications J. Photochem. Photobiol. B 98 77–94 [PubMed: 20031443]

Lihong H-IW and Wang V 2007 Biomedical Optics: Princoples and Imaging 1st edn (New York: Wiley)

Lin Y, Barber WC, Iwanczyk JS, Roeck W, Nalcioglu O and Gulsen G 2010a Quantitative fluorescence tomography using a combined trimodality FT/DOT/XCT system Opt. Express 18 7835–50 [PubMed: 20588625]

Lin Y, Barber WC, Iwanczyk JS, Roeck WW, Nalcioglu O and Gulsen G 2010b Quantitative fluorescence tomography using a trimodality system: *in vivo* validation J. Biomed. Opt 15 040503 [PubMed: 20799770]

Lin Y, Ghijsen M, Nalcioglu O and Gulsen G 2012a *In vivo* validation of quantitative frequency domain fluorescence tomography J. Biomed. Opt 17 126021 [PubMed: 23323291]

Lin Y, Kwong TC, Bolisay L and Gulse G 2012b Temperature-modulated fluorescence tomography based on both concentration and lifetime contrast J. Biomed. Opt 17 056007 [PubMed: 22612130]

Lin Y, Nouizi F, Kwong TC and Gulsen G 2015 Simulation-based evaluation of the resolution and quantitative accuracy of temperature-modulated fluorescence tomography Appl. Opt 54 7612–21 [PubMed: 26368884]

Liu F, Liu X, Zhang B and Bai J 2012 Extraction of target fluorescence signal from *in vivo* background signal using image subtraction algorithm Int. J. Autom. Comput 9 232–6

Lu Y, Zhu B, Darne CD, Tan I-C, Rasmussen JC and Sevick-Muraca EM 2011 Improvement of fluorescence-enhanced optical tomography with improved optical filtering and accurate model-based reconstruction algorithms J. Biomed. Opt 16 126002 [PubMed: 22191919]

Ma X, Van VP, Kimm MA, Prakash J, Kessler H, Kosanke K, Feuchtinger A, Aichler M, Gupta A and Rummeny EJ 2017 Integrin-targeted hybrid fluorescence molecular tomography/x-ray computed tomography for imaging tumor progression and early response in non-small cell lung cancer Neoplasia 19 8–16 [PubMed: 27940248]

Marshall MV, Rasmussen JC, Tan I-C, Aldrich MB, Adams KE, Wang X, Fife CE, Maus EA, Smith LA and Sevick-Muraca EM 2010 Near-infrared fluorescence imaging in humans with indocyanine green: a review and update Open Surgical Oncol. J 2 12

Nouizi F, Chabrier R, Torregrossa M and Poulet P 2009 3D modeling for solving forward model of no-contact fluorescence diffuse optical tomography method European Conf. on Biomedical Optics, Int. Society for Optics and Photonics (Munich, Germany) 7369_0C

Nouizi F, Erkol H, Luk A, Unlu MB and Gulsen G 2016a Real-time photo-magnetic imaging Biomed. Opt. Express 7 3899–904 [PubMed: 27867701]

Nouizi F, Kwong TC, Cho J, Lin Y, Sampathkumaran U and Gulsen G 2015a Implementation of a new scanning method for high-resolution fluorescence tomography using thermo-sensitive fluorescent agents Opt. Lett 40 4991–4 [PubMed: 26512501]

Nouizi F, Kwong TC, Kwong J, Cho J, Chan Y, Sampathkumaran U, Zhu Y, Alam MM and Gulsen G 2015b Excitation light leakage suppression using temperature sensitive fluorescent agents Proc. SPIE 9319 93190Y

Nouizi F, Luk A, Thayer D, Lin Y, Ha S and Gulsen G 2016b Experimental validation of a high-resolution diffuse optical imaging modality: photomagnetic imaging J. Biomed. Opt 21 16009 [PubMed: 26790644]

Ntziachristos V 2006 Fluorescence molecular imaging Annu. Rev. Biomed. Eng 8 1–33 [PubMed: 16834550]

Rice WL, Shcherbakova DM, Verkhusha VV and Kumar AT 2015 In vivo tomographic imaging of deep-seated cancer using fluorescence lifetime contrast Cancer Res. 75 1236–43 [PubMed: 25670171]

Roy R and Sevick-Muraca E 1999a Truncated Newton's optimization scheme for absorption and fluorescence optical tomography: part I theory and formulation, Opt. Express 4 353–71 [PubMed: 19396292]

Roy R and Sevick-Muraca E 1999b Truncated Newton's optimization scheme for absorption and fluorescence optical tomography: part II reconstruction from synthetic measurements Opt. Express 4 372–82 [PubMed: 19396293]

Sevick-Muraca E 2012 Translation of near-infrared fluorescence imaging technologies: emerging clinical applications Annu. Rev. Med 63 217–31 [PubMed: 22034868]

Sexton K, Davis SC, McClatchy D, Valdes PA, Kanick SC, Paulsen KD, Roberts DW and Pogue BW 2013 Pulsed-light imaging for fluorescence guided surgery under normal room lighting Opt. Lett 38 3249–52 [PubMed: 23988926]

Soubret A and Ntziachristos V 2006 Fluorescence molecular tomography in the presence of background fluorescence Phys. Med. Biol 51 3983 [PubMed: 16885619]

Tichauer KM, Holt RW, El-Ghussein F, Davis SC, Samkoe KS, Gunn JR, Leblond F and Pogue BW 2013 Dual-tracer background subtraction approach for fluorescent molecular tomography J. Biomed. Opt 18 016003

Tichauer KM, Holt RW, Samkoe KS, El-Ghussein F, Gunn JR, Jermyn M, Dehghani H, Leblond F and Pogue BW 2012 Computed tomography-guided time-domain diffuse fluorescence tomography in small animals for localization of cancer biomarkers J. Vis. Exp 65 e4050

Venugopal V, Chen J, Lesage F and Intes X 2010 Full-field time-resolved fluorescence tomography of small animals Opt. Lett 35 3189–91 [PubMed: 20890329]

Zhang Y, Zhang L, Yin G, Ma W and Gao F 2018 Assessing indocyanine green pharmacokinetics in mouse liver with a dynamic diffuse fluorescence tomography system J. Biophotonics 11 e201800041 [PubMed: 29797547]

Zhu B, Rasmussen JC, Lu Y and Sevick-Muraca EM 2010 Reduction of excitation light leakage to improve near-infrared fluorescence imaging for tissue surface and deep tissue imaging Med. Phys 37 5961–70 [PubMed: 21158309]
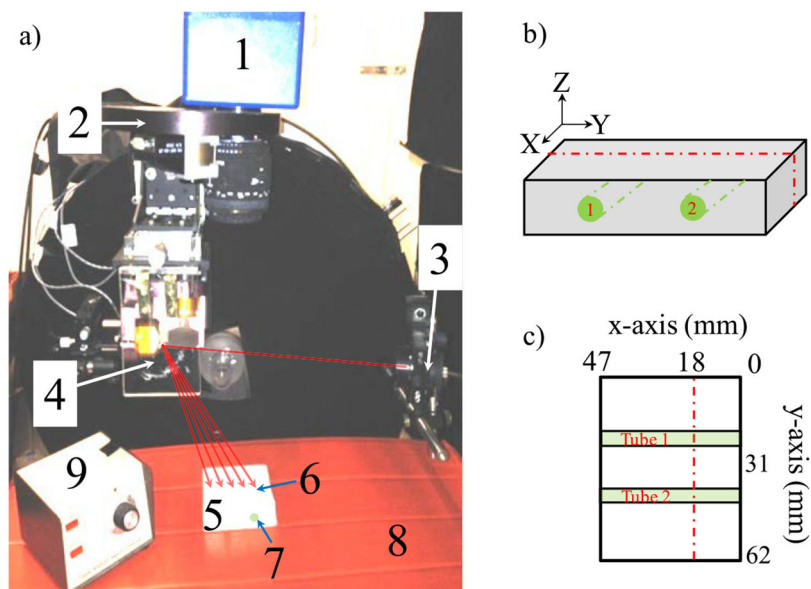
Figure 1.
(a) The instrumentation: (1) CCD camera, (2) filter wheel, (3) light source fiber, (4) galvano-mirrors, (5) agar phantom, (6) laser point illumination, (7) position of the inclusion and thermocouple tip, (8) heating pad and (9) temperature controller. In order to fully demonstrate the efficacy of our method in suppressing excitation leakage, the FT system was set up in reflection mode which yields a higher leakage of the excitation light. Schematic showing the used agar phantom, the tubes containing the ThermoDots and the laser scanning line (red dashed line): (b) side-view and (c) top-view.
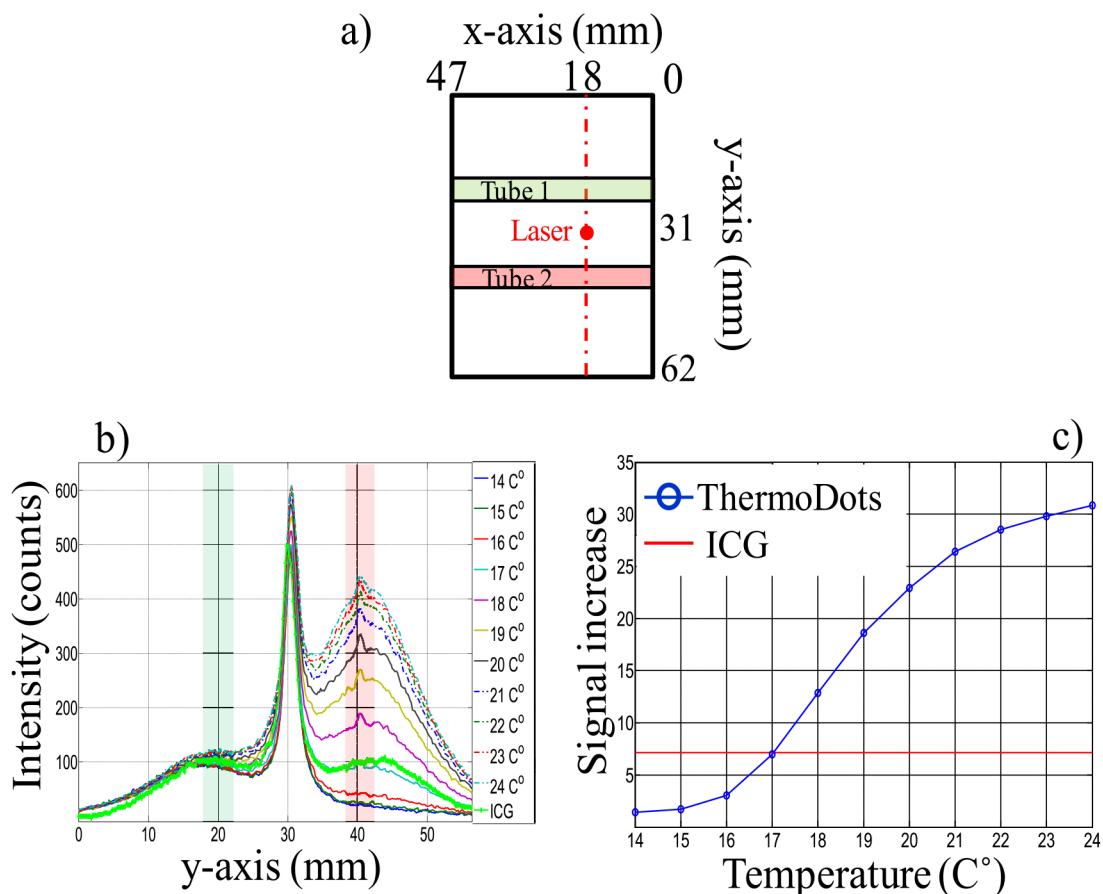
Figure 2.
(a) Top view of the phantom showing the two tubes and the position where the profiles are carried-out. (b) Profiles of the fluorescence light obtained during the characterization of ThermoDots. The green and red highlighted areas show the position of the ICG and ThermoDots tubes, respectively. (c) Integral of the fluorescence signals performed at ROIs above the two tubes.
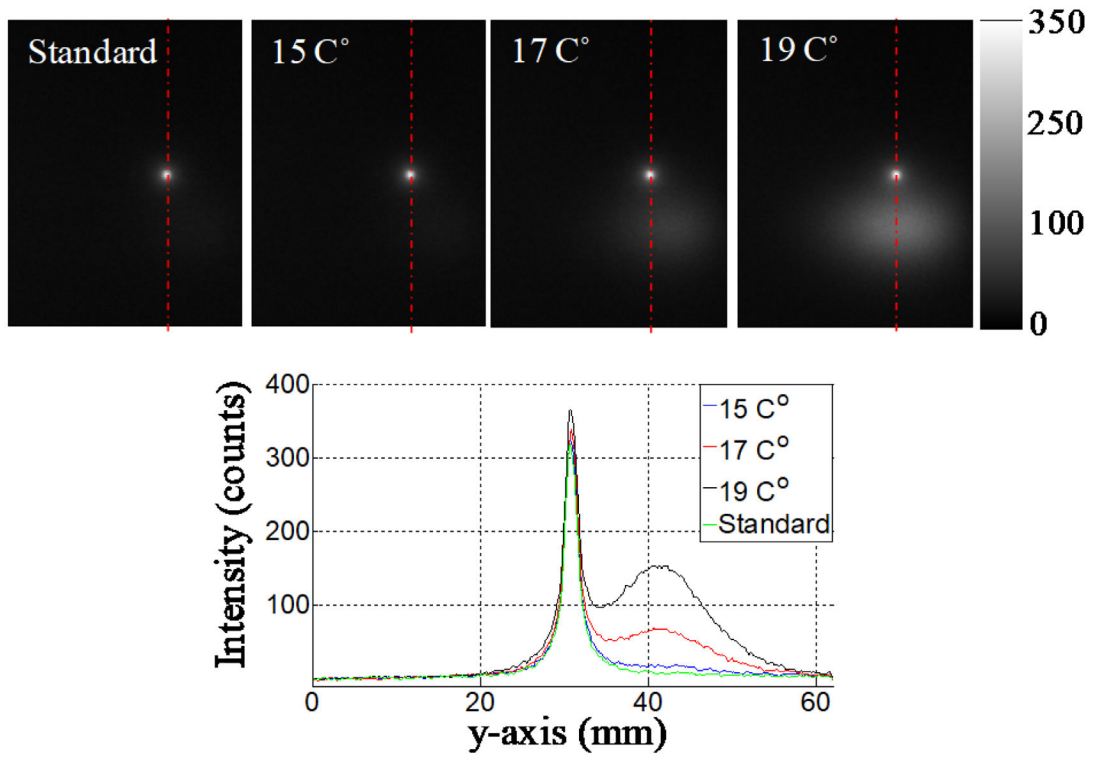
Figure 3.
The fluorescence images acquired using the *Standard method* and when ThermoDots are present within phantom at $T_1 = 15\ °C$, $T_2 = 17\ °C$ and $T_3 = 19\ °C$ are presented in the first row. The figure in the second row depicts the profiles along the dashed red lines.
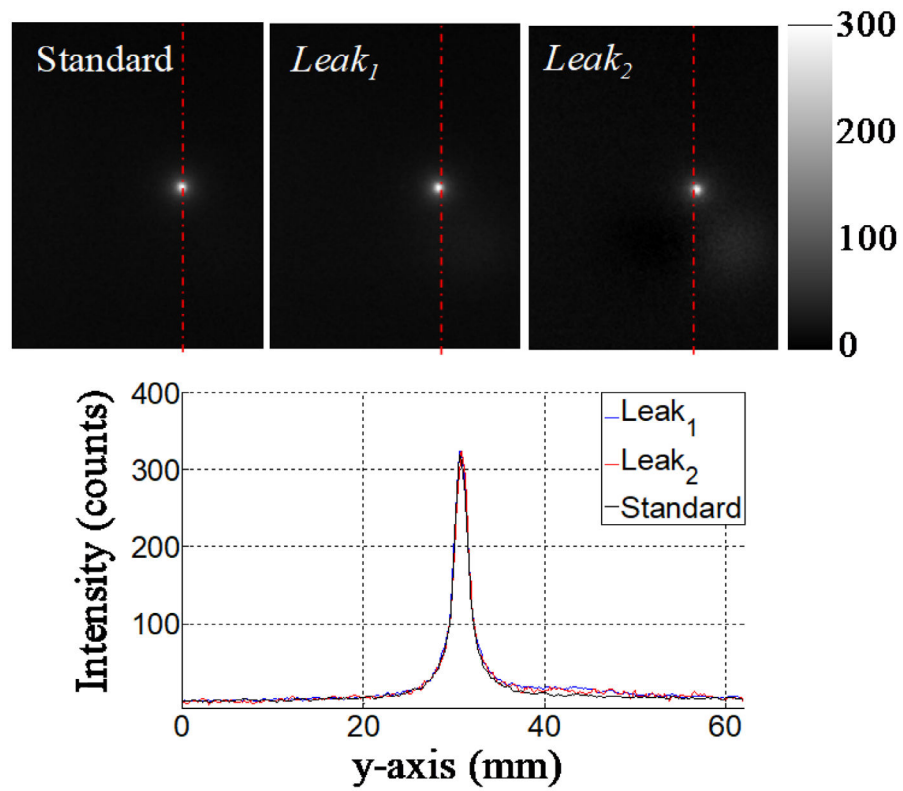
Figure 4.
The excitation light leakage measured using the *Standard method* (Standard), method 1 (*Leak₁*), and method 2 (*Leak₂*) are presented in the first row. The profiles along the dashed red line are presented in the second row.
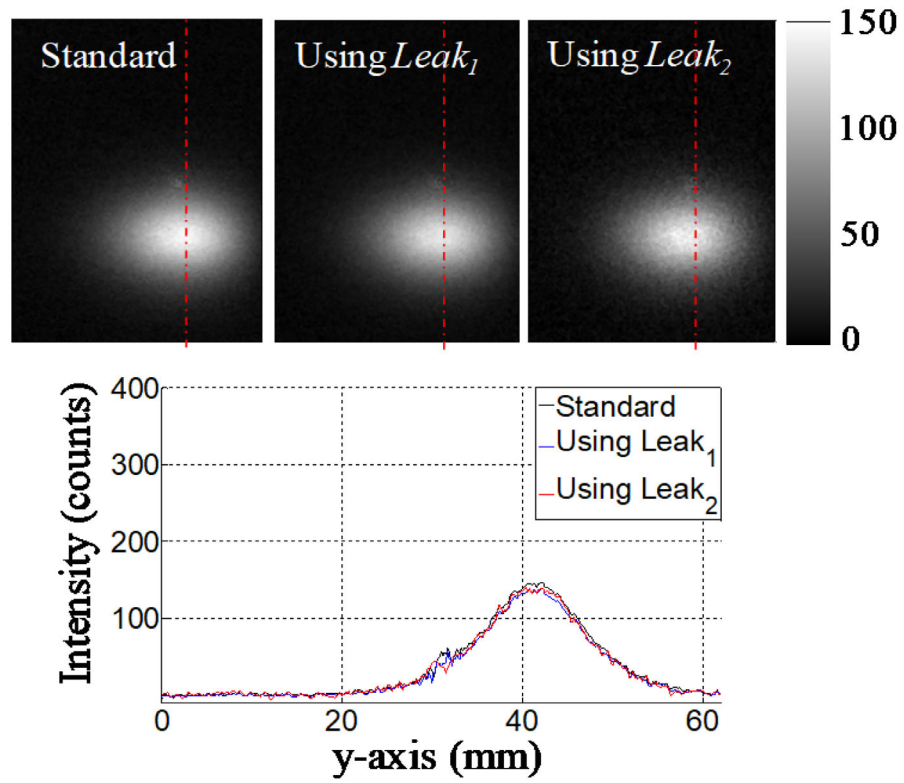
Figure 5.
The fluorescence data acquired at $T_3 = 19\ °C$ corrected using the *Standard method* (Standard), method 1 (*Leak_1*), and method 2 (*Leak_2*) are presented in the first row. The profiles along the dashed red line are presented in the second row.
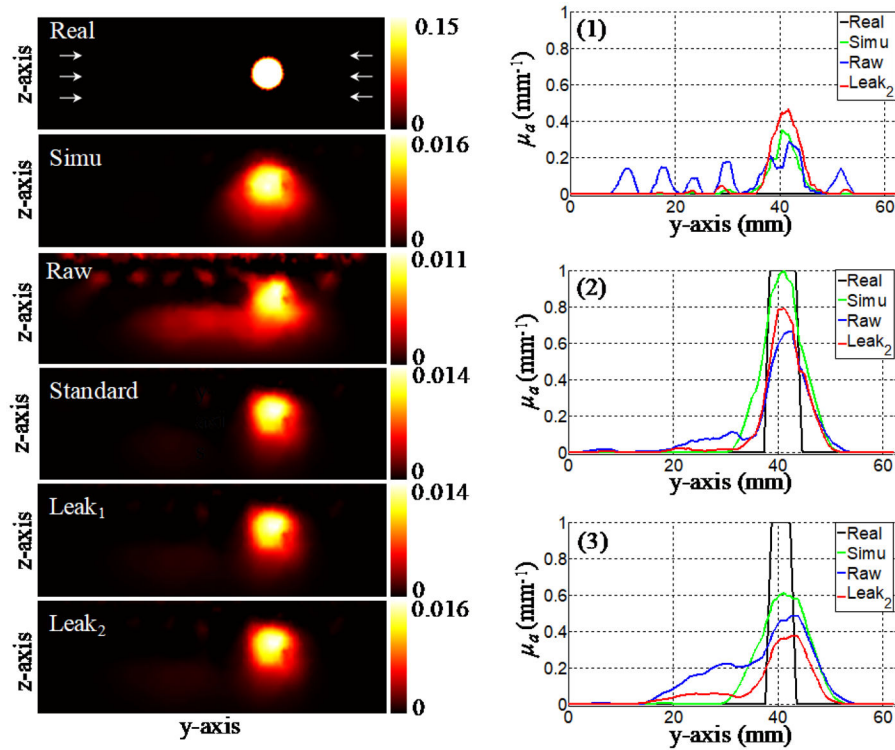
Figure 6.
The real fluorescence absorption (**Real**). The reconstructed fluorescence absorption images using: simulated data (**Simu**), raw data (**Raw**), and the corrected data using: *Standard method* (**Standard**), method 1 (**Leak₁**), method 2 (**Leak₂**). In figure, (1)–(3) represent the normalized profiles of the absorption fluorescence (μ_{af}) along the lines defined by the arrows 1, 2 and 3 on the Real image, respectively. The ratio between the reconstructed profiles is preserved by normalizing them to the maximum of the reconstructed images using simulated data (**Simu**).

Table 1.

Summary of the mean value and standard deviation of the reconstructed fluorescence absorption, μ_{af} (mm^{-1}).

	Simu	**Raw**	**Standard**	**Leak$_1$**	**Leak$_2$**
Background	0.0003 ± 0.0012	0.0005 ± 0.0009	0.0003 ± 0.0008	0.0003 ± 0.0008	0.0003 ± 0.0001
Inclusion	0.0122 ± 0.0025	0.0057 ± 0.0013	0.0089 ± 0.0031	0.0091 ± 0.0034	0.0105 ± 0.0035